PHYSICAL REVIEW E **85**, 020301(R) (2012)

Bottlenecks in granular flow: When does an obstacle increase the flow rate in an hourglass?

F. Alonso-Marroquin,[1,*] S. I. Azeezullah,[1,2] S. A. Galindo-Torres,[3] and L. M. Olsen-Kettle[4]
[1]*School of Civil Engineering, The University of Sydney, Sydney, New South Wales 2006, Australia*
[2]*School of Mathematics and Physics, The University of Queensland, St. Lucia, Queensland 4072, Australia*
[3]*School of Civil Engineering, The University of Queensland, St. Lucia, Queensland 4072, Australia*
[4]*School of Earth Sciences, The University of Queensland, St. Lucia, Queensland 4072, Australia*
(Received 10 February 2011; revised manuscript received 24 November 2011; published 22 February 2012)

Bottlenecks occur in a wide range of situations from pedestrians, ants, cattle, and traffic flow to the transport of granular materials. We examine granular flow across a bottleneck using simulations of monodisperse disks. Contrary to expectations but consistent with previous work, we find that the flow rate across a bottleneck actually increases if an obstacle is optimally placed before it. Using the hourglass theory and a velocity-density relation, we show that the peak flow rate corresponds to a transition from free flow to congested flow, similar to the phase transition in traffic flow.

DOI: 10.1103/PhysRevE.85.020301 PACS number(s): 45.70.Mg, 45.70.Vn, 47.57.Gc

The improvement in flow rate of particles passing through a bottleneck has applications ranging from industrial granular flow [1,2] and traffic flow [3] to escape dynamics under panic [4]. Optimal design for the conveyance and storage of powders and bulk solids is a challenge faced by nearly all industries, from powder coating to food, from nanoscale powders and pharmaceuticals to cement, coal, and ore [5]. Since the 1960's, empirical placement of inserts (obstacles) before outlet openings has been used in silo design for a number of reasons, including transformation of the flow profile from funnel flow to mass flow, enlargement of the mass flow rate, reduction of the stresses in the silo, and mixing and homogenizing of bulk solids [1,2,5]. If the obstacle is placed at an optimal height, it disturbs arches that block the flow from being created and becoming stable [6]. Whereas the flow problems frequently found in silo flow are relatively well known, improvements to design of optimized escape routes for panicking crowds are at their inception.

Studies on escape dynamics under panic have shown that obstacles placed before the outlet can lead to substantial changes in flow patterns. Due to the difficulties in performing real experiments with humans, simulations of self-driven particles have been proposed. These simulations have already shown, counterintuitively, the benefit of placing an obstacle before an exit to prevent or reduce injuries under conditions of panicked escape [4,7]. Placing a column in front of an exit substantially reduced evacuation time for ants squirted with citronella [8,9]. Escobar and De la Rosa explain this behavior as the "waiting-room" effect [7] whereby particles slow down and accumulate above the obstacle, decongesting the exit and increasing the flow rate. In this Rapid Communication we provide full modeling of the flow of monodisperse granular material around such an obstacle where we observe a peak in flow rate for optimized conditions. Based on statistics from simulations, we develop a consistent framework that characterizes the relationship between the flow rate and the position and size of the obstacle.

We present a parametric study from a statistical analysis of thousands of simulations of gravity-driven granular flow through an hourglass hopper. We place a circular obstacle above the bottleneck and investigate how it affects the flow rate. All simulations consider circular particles passing through a neck of width D_0 of an hourglass-shaped hopper with angle θ with respect to the vertical, as shown in Fig. 1. A circular obstacle of diameter D is placed centrally at a distance H above the bottleneck. Initially the particles are placed at the top of the hourglass. Gravity ensures that the particles flow through the bottleneck. We enforce periodic boundary conditions by replacing the particles that have reached the bottom back to the top of the hopper. The average number of refilling particles per second (mass flow rate over particle mass) is used to measure the flow rate J.

The particles interact with each other via elastic, viscous, and frictional forces, and are subject to gravity. Details of the particle-based model are presented in Ref. [10]. The parameters of the model and their units are as follows: normal and tangential contact stiffness k_n (N/m) and k_t (N/m), friction coefficient μ, normal and tangential coefficients of viscosity γ_n (1/s) and γ_t (1/s), particle mass m (kg), particle diameter d (m), and gravity g (m/s^2). The dimensionless flow rate J/J_0 is given as a function of the geometrical parameters θ, D/d, D_0/d, and the contact parameters μ, $a_0 = \omega_0/\gamma_n$, $a_1 = k_t/k_n$, $a_2 = \gamma_t/\gamma_n$, and $a_3 = \omega_0/J_0$, where $J_0 = (g/d)^{1/2}$ and $\omega_0 = (k_n/m)^{1/2}$. The contact parameters were chosen as follows: $a_0 = 0.71$ gives a restitution coefficient of 0.04 [11]; $a_1 = a_2 = 0.1$ leads to a Poisson ratio of 0.3 for a hexagonal packing [12]; $a_3 = 0.005$ guarantees overlaps of lower than 5% of the particle diameter; and $\mu = 0.2$. The default geometrical parameters are $D_0 = 6.3d$, which is wide enough to avoid clogging, $H/d = D/d = 9.46$, and $\theta = 30^\circ$. Each simulation runs for $34\,000t_c$, where $t_c = 2\pi/\omega_0$ is the characteristic collision time. The system consists of 1670 particles, which is enough to guarantee steady flow and a filling height larger than three times the neck diameter; we observed little variation in flow rate with a change in the number of particles.

Simulations with no obstacle showed that the flow rate depends on the neck diameter, according to the Beverloo

*fernando.alonso@sydney.edu.au

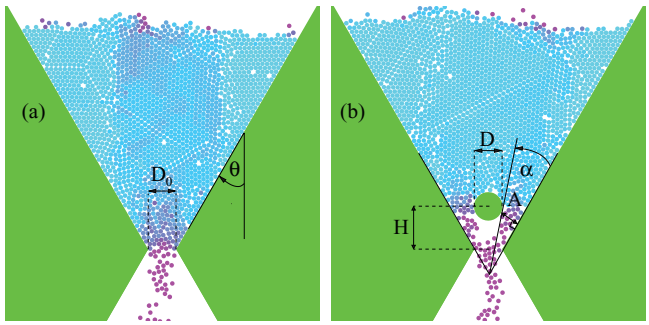

FIG. 1. (Color online) Snapshot of the simulation of gravity-driven granular flow with no obstacle (a), and with an obstacle of $6.3d$ diameter (b). The color encodes particle speed (darker is faster). The parameters governing the flow are hopper angle θ, bottleneck width D_0, angle of convergence α, and aperture A created by the obstacle.

relation that is derived from the hourglass theory [13]:

$$\frac{J}{J_0} = C\frac{(D_0/d - c_0)^{\beta}}{\sin^{1/2}\theta}, \quad J_0 = (g/d)^{1/2}, \tag{1}$$

where $\beta = 3/2$ for two-dimensional (2D) flow [14], and $C = 1.4$ and $c_0 = 3.2$ are fitting parameters as shown in Fig. 2, the latter one reflecting the transition from jamming to continuous flow. To investigate the effect on the obstacle on the flow rate, we fixed the neck diameter to $D_0 = 6.3d$, which leads to continuous flow when no obstacle is present.

Two series of simulations are performed to investigate the effect of placing an obstacle on the flow rate. In the first series we fixed the height of the center of the obstacle to $9.46d$ above the center of the bottleneck and varied its diameters. Figure 3(a) shows the flow rate versus obstacle diameter D for different hopper angles θ. For each θ the flow rate peaks at a finite value of obstacle diameter that we call the optimal diameter. As the angle of the hopper increases from 26° to 55°, the optimal diameter increases while the peak flow rate decreases. In the second series of simulations we investigate how the flow rate depends on the height of the obstacle. We fixed the diameter of the obstacle to $9.46d$ and varied the height H. The results are shown in Fig. 3(b). For each hopper angle there is an optimal height for which the flow rate is maximal. Again, as the angle of the hopper increases, the peak decreases, and the optimal height becomes smaller. The main difference between both cases is that, when the height of the obstacle is varied, a higher flow rate is reached than when changing its

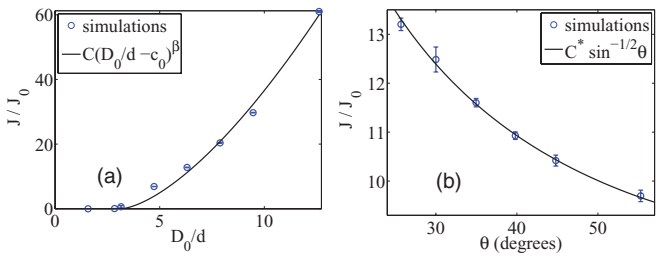

FIG. 2. (Color online) Flow rate without obstacle vs neck width in (a), and vs hopper angle using $C^* = C(D_0/d - c_0)$ in (b); the best fit is in agreement with the Beverloo relation, Eq. (1).

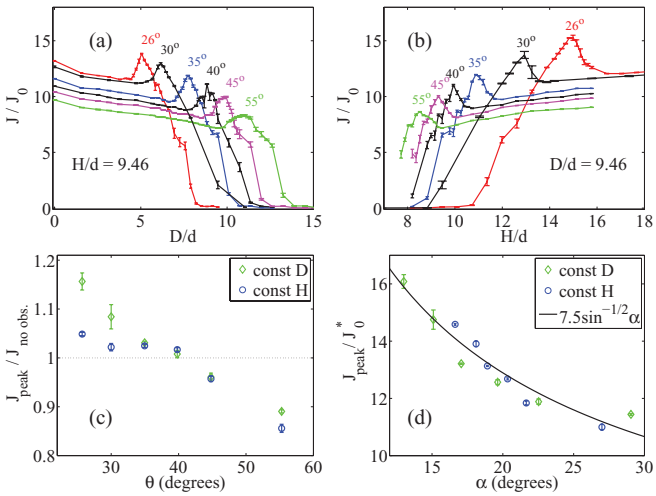

FIG. 3. (Color online) Flow rate vs obstacle diameter in (a), and vs obstacle height in (b), for different values of hopper angle θ. In (a) the center of the obstacle is $9.46d$ above the center of the neck. In (b) the obstacle diameter is $9.46d$. Differences in initial conditions cause statistical fluctuations, so for each parameter suite the simulation was repeated 32 times with the particles in different initial positions. The error bars indicate standard errors. In (c) we show the ratio between the peak flow rate and the flow rate without an obstacle vs hopper angle θ for both cases. The peak flow rate vs angle of convergence is fitted in (d) using the Beverloo relation with effective gravity $g^* = g\cos\theta$.

diameter. The ratio between flow rate at peak with an obstacle and flow rate without an obstacle is shown in Fig. 3(c). For a hopper angle of 26° there is a 5% improvement of flow rate for the optimal diameter, while it improves 16% when the height is optimized.

The main conclusion of these two series of simulations is that for hopper angles below 40° there is only a very narrow, specific range of heights and diameters of the obstacle where the flow rate is higher than that the flow rate without an obstacle. More support and evidence for the optimized flow rate due to obstacle placement before an outlet opening can be found from numerical simulations of panic-driven pedestrians [4], experiments with ants [9], and more practically in cattle herding where the stockman has the role of the obstacle [8]. The contribution of our simulations is to show that obstacle placement needs to be optimized for improvement in the flow rate.

Now we question whether or not the hourglass theory can be used to describe the dependency of the flow rate on the height and the diameter of the obstacle. Figure 1(b) shows two important control parameters for the flow rate with an obstacle. The first one is the aperture, which is defined as the minimum distance between the obstacle and the hopper wall. The second one is the angle of convergence α. We extend the lines of the walls to meet at the apex below the bottleneck, and then we draw a line tangent to the obstacle passing through the apex. α is the angle between this line and the extended line of the nearer wall. Simulations show that the optimized obstacle splits the bottleneck into two smaller hoppers on either side of the obstacle. This decreases the effective hopper angle, enabling an improvement on the flow rate according to Eq.

(1). Let us assume that each one of the hoppers has an angle α, and that the particles are driven by an effective gravity of $g^* = g\cos\theta$. Using Eq. (1) these two assumptions lead to $J/J_0^* = C^* \sin^{-1/2}\alpha$, where $J_0^* = (g^*/d)^{1/2}$. Figure 3(d) plots the peak flow rate versus the angle of convergence for simulations with constant obstacle diameter and height. We found good agreement with the hourglass theory. This proves that the main benefit of the obstacle is to produce a less convergent flow, which leads to higher flow rates.

But the convergence angle is not the only parameter controlling the flow rate. The variation of the flow rate around its peak value is governed by the aperture, i.e., the distance between the obstacle and the hopper wall. If the aperture is too narrow, the particles get clogged, leading to a decrease of the flow rate; if the aperture is too wide, the space between the obstacle and the bottleneck gets congested, leading to a flow rate lower than the flow rate without an obstacle. Between these two regimes there is a narrow range of apertures that produce the waiting-room effect [7], with reduction of density above the bottleneck and a subsequent increase in the velocity of particles, and therefore in flow rate.

The hourglass theory assumes the density as a constant parameter of the problem, so that it cannot be used to capture this waiting-room effect. We will extend this theory by constructing a microscopic traffic-flow model that describes the dependency of the density, velocity, and flow rate with the aperture. Traffic-flow modeling assumes that in the steady state the mean velocity V of the particles (car or pedestrians) is a function of the density ρ [3,15]. The flow-rate density (mass flow rate per area) is calculated as the product of the density and the normal velocity, $j = \rho V$, which implies a dependence of the flow solely on the density. For the hourglass the flow rate (particles crossing the bottleneck per second) is the integral of the flow-rate density over the bottleneck area D_0 divided by the particle mass m. This leads to $J = \bar{j} D_0/m$, where $\bar{j}$ is the mean value of j over the bottleneck. Now we will assume that the fluctuations of density and velocity at the bottleneck are uncorrelated, so that $\overline{\rho V} = \bar{\rho}\bar{V}$. Under this *uncorrelation hypothesis*, the flow rate may be approximated by that which we call the microscopic flow rate:

$$J_{\mathrm{mic}} = \bar{\rho}\bar{V} D_0/m. \qquad (2)$$

We will check the validity of this hypothesis. First, the mean values of density and velocity are calculated by using a rectangular area $0.025 D_0$ above and below the bottleneck. The density is calculated as the mass of particles in this rectangle divided by its area. The mean velocity is the average or the vertical velocity of the particles over this rectangle. Confident values of these two quantities are obtained by averaging over 800 snapshots of the simulation. The velocity and density are normalized by $V_0 = (gd)^{1/2}$ and $\rho_0 = 2\cot 60^\circ m d^{-2}$, the latter being the density of a hexagonal packing.

Figures 4(a) and 4(c) show the time average of both mean density and mean velocity versus aperture. We can distinguish three flow regimes: Zone I corresponds to apertures below $4.3d$. In this zone the region between the bottleneck and the obstacle is loosely packed and the particles are relatively free and unconstrained. This regime is characterized by an increase of the velocity as the density increases. This is similar

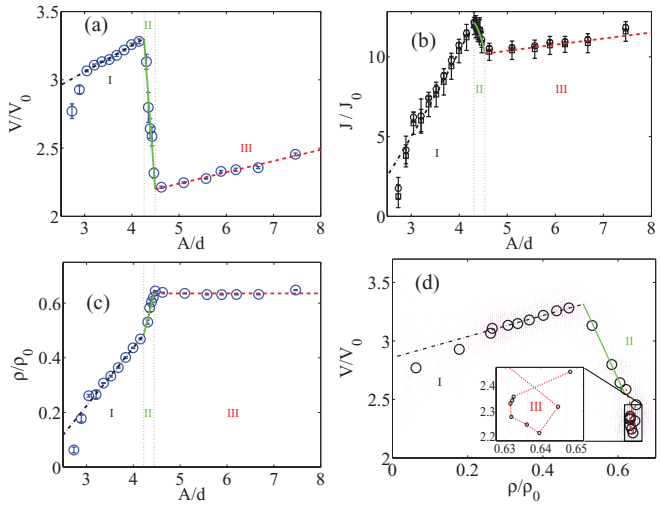

FIG. 4. (Color online) Mean velocity (a) and mean density (d) at the bottleneck vs aperture. The lines show the multilinear fit of the data. The squares in (b) show the flow rate J vs aperture calculated as the number of refilling particles per second. The circles in (b) show the microscopic flow rate J_{mic} calculated from Eq. (2). The lines in (b) correspond to the model using the fitting in (a) and (c). Each dot in (d) shows the mean velocity vs mean density in a snapshot of the simulation. The circles show the time average of both density and velocity at different apertures. The bilinear fitting is performed using the slopes obtained from zones I and II in (a) and (c). Zone III corresponds to the hysteresis loop shown in the inset.

to the *free-flow* regime in traffic flow, where an increase in the density of cars leads to an increase in flow rate.

Zone II corresponds to an aperture of $4.3d$–$4.5d$. We call this regime the *congested zone*, because it resembles the regime in vehicular flow where a further increase in the density of cars leads to an abrupt decrease of the mean velocity. The transition between zones I and II is where the waiting-room effect takes place, leading to peak flow rates. This effect is characterized by a change in the relationship between velocity and density. While the density is still increasing with an increase of aperture, the velocity in this zone changes from increasing to decreasing due to congestion at the bottleneck.

A different transition is observed around $A = 4.5d$. When the aperture passes this value the density stops increasing and reaches a constant value $\rho_{\max} = 0.64\rho_0$, while the velocity changes from decreasing to increasing. This corresponds to zone III, which we call a *non-Markovian* zone, because there the mean velocity does not depend on density but on the history of particles. Here the particles crossing the bottleneck "remember" whether they collided with the obstacle, because if they did, their velocity is lower than if they had not collided.

The three regimes can be fitted using a multilinear relation of velocity and density versus aperture. These relations, along with Eq. (2), are then used to calculate the dependency of microscopic flow rate on aperture, as shown in Fig. 4(b). We see that the microscopic flow rate J_{mic} is close to the flow rate J given by the number of refilling particles per second. This supports the validity of the uncorrelation hypothesis used to derive Eq. (2).

The optimal aperture corresponds to the point where the congested zone (zone II) and free-flow zone (zone I) meet.

This shows that the waiting-room effect resembles the phase transition observed in vehicular traffic. This transition is presented in Fig. 4(d). We can recognize the transition at around $(V_c, \rho_c) = (3.3V_0, 0.51\rho_0)$. The best fit of our velocity-density relation is a bilinear relation, which can be used to express the flow rate around the peak value as $J/J_{\text{peak}} = (\bar{\rho}/\rho_c)[\bar{V}(\bar{\rho})/V_c]$. Since the flow rate at the peak was given by $J_{\text{peak}} = C^*(g\cos\theta/d)^{1/2}\sin^{-1/2}\alpha$, the dependency of the flow rate around the peak can be expressed as

$$J = C^*\sqrt{\frac{g\cos\theta}{d\sin\alpha}}\,\frac{\bar{\rho}(A)\bar{V}[\bar{\rho}(A)]}{\rho_c V_c}, \tag{3}$$

where $\bar{\rho}(A)$ and $\bar{V}(\bar{\rho})$ were fitted in Figs. 4(b) and 4(d). We note that this bilinear velocity-density relation is in stark contrast to previous models of traffic flow where the velocity-density relation is monotonically decreasing [15]. This difference appears due to the presence of particle-obstacle collisions in the former and a lack thereof in the latter. Also note that such a velocity-density relation with two regimes does not capture the additional transition from the congested to the non-Markovian regime mentioned above. In the latter regime the velocity depends on aperture rather than density, which stays constant around $\rho_{\max}$. This regime is characterized by minute hysteresis loops in the velocity-density relation. These loops differ from the ones observed in traffic flow, which lead to a return transition from congested flow to free flow [16]. It is interesting and unexpected to observe such hysteresis loops with this completely deterministic model of gravity-driven particles.

To conclude, we have shown that an obstacle in an hourglass can increase the flow rate by up to 16%. The optimized obstacle splits the flow into two less convergent hopper flows. Here the relation between peak flow rate and the angle of convergence is consistent with the $\sin^{-1/2}$ relation predicted by the hourglass theory. The phenomenology of the waiting-room effect was described as a transition from free flow to congested flow that fits well to a bilinear velocity-density relation.

We thank M. Burd, N. Shiwakoti, A. Ramirez, I. Zuriguel, B. Pailthorpe, and J. D. Muñoz-Castaño for support and helpful discussions. Computations were performed on the Australian Earth Systems Simulator. L.M.O. is grateful for the support from the University of Queensland's ResTeach project.

[1] J. Johanson and W. Kleysteuber, Chem. Eng. Prog. **62**, 79 (1966).
[2] J. Johanson, Bulk Solids Handl. **2**, 495 (1983).
[3] D. Helbing, A. Johansson, J. Mathiesen, M. H. Jensen, and A. Hansen, Phys. Rev. Lett. **97**, 168001 (2006).
[4] D. Helbing, I. Farkas, and T. Vicsek, Nature (London) **407**, 487 (2000).
[5] D. Schulze, *Powders and Bulk Solids* (Springer, Berlin, 2008).
[6] I. Zuriguel, A. Janda, A. Garcimartín, C. Lozano, R. Arévalo, and D. Maza, Phys. Rev. Lett. **107**, 278001 (2011).
[7] R. Escobar and A. De La Rosa, in *Advances in Artificial Life, Proceedings of the 7th European Conference, ECAL 2003*, Dortmund, Germany, September 14–17, 2003, edited by W. Banzhaf *et al.*, Lecture Notes in Computer Science Vol. 2801 (Springer, Berlin, 2003), pp. 97–106.
[8] N. Shiwakoti, M. Sarvi, G. Rose, and M. Burd, Transp. Res. Rec. **2137**, 31 (2009).
[9] M. Burd, N. Shiwakoti, M. Sarvi, and G. Rose, Ecol. Entomol. **35**, 464 (2010).
[10] F. Alonso-Marroquín and Y. Wang, Granular Matter **11**, 317 (2009).
[11] S. Luding, H. J. Herrmann, and A. Blumen, Phys. Rev. E **50**, 3100 (1994).
[12] Y. Wang and P. Mora, J. Mech. Phys. Solids **56**, 3459 (2008).
[13] R. Nedderman, *Statics and Kinematics of Granular Materials* (Cambridge University Press, Cambridge, UK, 2005).
[14] C. Mankoc, A. Janda, R. Arévalo, J. Pastor, I. Zuriguel, A. Garcimartín, and D. Maza, Granular Matter **9**, 407 (2007).
[15] M. Treiber, A. Hennecke, and D. Helbing, Phys. Rev. E **59**, 239 (1999).
[16] B. Kerner, *Introduction to Modern Traffic Flow Theory and Control: The Long Road to Three-Phase Traffic Theory* (Springer, Berlin, 2009).